Structure and Properties of a Complex of alpha-Synuclein and a Single-Domain Camelid Antibody

De Genst, Erwin; Guilliams, Tim; Wellens, Joke; O'day, Elizabeth M.; Waudby, Christopher A.; Meehan, Sarah; Dumoulin, Mireille; Hsu, Shang-Te Danny; Cremades, Nunilo; Verschueren, Koen; Pardon, Els; Wyns, Lode; Steyaert, Jan; Christodoulou, John; Dobson, Christopher M.

Published in:
Journal of Molecular Biology

DOI:
10.1016/j.jmb.2010.07.001

Publication date:
2010

Document Version:
Final published version

doi:10.1016/j.jmb.2010.07.001 J. Mol. Biol. (2010) 402, 326–343

JMB

Available online at www.sciencedirect.com

ScienceDirect

ELSEVIER

Structure and Properties of a Complex of α-Synuclein and a Single-Domain Camelid Antibody

Erwin J. De Genst[1,2], Tim Guilliams[1]†, Joke Wellens[2,3]†, Elizabeth M. O'Day[1,2]†, Christopher A. Waudby[1,2], Sarah Meehan[1], Mireille Dumoulin[1,2], Shang-Te Danny Hsu[1], Nunilo Cremades[1], Koen H.G. Verschueren[2,3], Els Pardon[2,3], Lode Wyns[2,3], Jan Steyaert[2,3], John Christodoulou[1,2] and Christopher M. Dobson[1]*

[1]*Department of Chemistry, University of Cambridge, Lensfield Road, Cambridge CB2 1EW, UK*

[2]*Structural Biology Brussels, Vrije Universiteit Brussel, Pleinlaan 2, B-1050 Brussels, Belgium*

[3]*Structural Biology Brussels, Department of Molecular and Cellular Interactions, Vlaams Instituut voor Biotechnologie, Pleinlaan 2, B-1050 Brussels, Belgium*

Received 1 March 2010; received in revised form 1 July 2010; accepted 2 July 2010
Available online 8 July 2010

The aggregation of the intrinsically disordered protein α-synuclein to form fibrillar amyloid structures is intimately associated with a variety of neurological disorders, most notably Parkinson's disease. The molecular mechanism of α-synuclein aggregation and toxicity is not yet understood in any detail, not least because of the paucity of structural probes through which to study the behavior of such a disordered system. Here, we describe an investigation involving a single-domain camelid antibody, NbSyn2, selected by phage display techniques to bind to α-synuclein, including the exploration of its effects on the *in vitro* aggregation of the protein under a variety of conditions. We show using isothermal calorimetric methods that NbSyn2 binds specifically to monomeric α-synuclein with nanomolar affinity and by means of NMR spectroscopy that it interacts with the four C-terminal residues of the protein. This latter finding is confirmed by the determination of a crystal structure of NbSyn2 bound to a peptide encompassing the nine C-terminal residues of α-synuclein. The NbSyn2:α-synuclein interaction is mediated mainly by side-chain interactions while water molecules cross-link the main-chain atoms of α-synuclein to atoms of NbSyn2, a feature we believe could be important in intrinsically disordered protein interactions more generally. The aggregation behavior of α-synuclein at physiological pH, including the morphology of the resulting fibrillar structures, is remarkably unaffected by the presence of NbSyn2 and indeed we show that NbSyn2 binds strongly to the aggregated as well as to the soluble forms of α-synuclein. These results give strong support to the conjecture that the C-terminal region of the protein is not directly involved in the mechanism of aggregation and suggest that

*Corresponding author. E-mail address: cmd44@cam.ac.uk.

† T.G., J.W. and E.M.O'D. contributed equally to this work.

Present addresses: E. O'Day, Chemical Biology Department, Harvard University, 12 Oxford Street, Cambridge, MA 02138, USA; C. Waudby and J. Christodoulou, Research Department of Structural and Molecular Biology, University College London, Darwin Building, Gower Street, London WC1E 6BT, UK; M. Dumoulin, Enzymologie et Repliement des Protéines, Centre d'Ingénierie des Protéines, Université de Liège, Institut de Chimie B6, 4000 Liège (Sart Tilman), Belgium.

Abbreviations used: IDP, intrinsically disordered protein; ITC, isothermal titration calorimetry; ANS, 1-anilino-8-naphthalene sulfonate; ThT, thioflavin T; TEM, transmission electron microscopy; ASA, solvent-accessible surface area; HSQC, heteronuclear single quantum coherence; CDR, complementarity-determining region; EM, electron microscopy; PBS, phosphate-buffered saline; PEG, polyethylene glycol; BSA, bovine serum albumin.

binding of NbSyn2 could be a useful probe for the identification of α-synuclein aggregation *in vitro* and possibly *in vivo*.

Keywords: α-synuclein; amyloid; nanobody; nuclear magnetic resonance; X-ray crystallography

Edited by K. Kuwajima

Introduction

Numerous studies have indicated that α-synuclein plays a crucial role in the development of Parkinson's disease and a number of related neurological disorders including dementia with Lewy bodies, multiple system atrophy, and the Lewy body variant of Alzheimer's disease.[1–6] It is very widely believed that the aggregation of α-synuclein to its alternative 'amyloid' state is a crucial aspect of all these disorders.[2–6] Moreover, and in common with a range of other neurological diseases, it is thought that pathogenesis results from the oligomeric precursors or fragments of the fibrillar amyloid state that are toxic and able to disrupt the function in particular of dopaminergic neurons.[1]

Human α-synuclein is a 140-residue intrinsically disordered protein (IDP) of unknown function, although there is increasing evidence that the protein is involved in vesicular axonal transport.[7] The aggregation behavior of α-synuclein has been widely studied *in vitro* and it is thought that self-association occurs initially to give a range of oligomeric species.[8–11] These oligomers can then aggregate further to generate protofibrils that eventually transform into mature amyloid fibrils. As discussed above, recent studies have suggested that the oligomeric species are highly toxic, perhaps through their ability to interact with and to disrupt membranes.[12–19]

The natively unfolded character of α-synuclein in its monomeric form, as well as the existence of an ensemble of oligomeric intermediates that are transiently populated during the aggregation process leading to fibril formation, makes it challenging to obtain structural details about individual species and to elucidate the molecular mechanisms of the process that lead to toxicity.[20] The use of specific molecular probes, such as antibodies, has, however, the potential to obtain such information in exquisite detail, because these can be raised to be selective not just for proteins in their native state but also for non-native states populated in the process of aggregation, including transient species such as small oligomers.[21] Of particular interest in this regard are camelid heavy-chain antibodies that lack the light chains of conventional antibodies and enable single-domain binding fragments to be obtained, species known as nanobodies.[22–26] Such nanobodies are small, highly stable and soluble, and easily expressed in large quantities but retain the high specificity and high affinity typical of conventional antibodies binding to their targets.[23–26] These qualities mean that nanobodies are extremely powerful as molecular probes of fibril formation using biophysical methods such as NMR and X-ray crystallography[27–29] and potentially as diagnostic and therapeutic reagents for amyloid diseases.[30,31]

As a result of the link between the aggregation of α-synuclein and Parkinson's disease, the ability of molecules and ions to enhance or inhibit the aggregation propensity of α-synuclein has been widely studied. Thus, for example, the binding of divalent cations has been shown to increase dramatically the rate of fibril formation by this protein,[32–35] as has the binding of polyamines.[36–40] In both cases, it is believed that the positively charged ions and molecules interact with the highly negatively charged C-terminal region of the α-synuclein sequence, reducing electrostatic repulsion and disrupting long-range interactions, hence leading to an increased ability to self-associate.[32–43] However, the disruption of long-range contacts might not be the most important factor that leads to enhanced fibril formation, as the disease-related variants do not show a significant reduction in long-range contacts, with the E46K variant actually enhancing the C-terminal to N-terminal contacts in α-synuclein.[44] The ability of α-synuclein to interact with larger molecules, including proteins, remains, however, largely unexplored and mainly limited to interactions with molecular chaperones.[45–47] One example, however, where detailed studies have been carried out involves the chaperone Hsp70, which has been shown to have the ability strongly to inhibit fibril formation by α-synuclein, through a mechanism that appears to involve binding to oligomeric species, thereby preventing them from undergoing further self-association.[46]

In this article, we describe detailed studies of the interaction of a nanobody, NbSyn2, with α-synuclein and of its effect *in vitro* on the aggregation properties of the latter. NMR spectroscopy and X-ray crystallography reveal that NbSyn2 binds to residues in the C-terminal region of α-synuclein. A range of biophysical studies shows that, although NbSyn2 binds tightly to α-synuclein, no significant structural changes can be detected within the α-synuclein molecule associated with its binding. Finally, the aggregation behavior of α-synuclein *in vitro* was found to be unaffected by the binding of the nanobody, a result that sheds light on the likely

structure of the fibrils and their precursors and on the mechanism by which proteins bind to IDPs.

Results

Secondary-structure changes and thermal stability measurements using CD spectroscopy

To assess the nature of any changes in secondary structure that occur to either component of the complex formed when NbSyn2 binds α-synuclein, we recorded far-UV spectra at 25 °C of the two proteins alone and together in equimolar quantities (Fig. 1a).

The circular dichroism (CD) spectrum of α-synuclein alone reflects its highly unstructured conformation, while NbSyn2 has a CD spectrum characteristic of a highly β-sheet-rich immunoglobulin fold,[48] with minima at both 215 and 229 nm and maxima at 222 and 202 nm. The CD spectrum of the NbSyn2:α-synuclein complex, after subtraction of the spectra of both the unbound α-synuclein and NbSyn2, shows that there is no significant secondary-structure perturbation to either component as a result of their interaction to form a bimolecular complex. In additional experiments, we were able to estimate the midpoint of the thermal unfolding (T_m) of the nanobody, by monitoring the change in CD signal at 222 nm as a function of temperature. We obtained a T_m value of 67±1 °C for NbSyn2 alone at

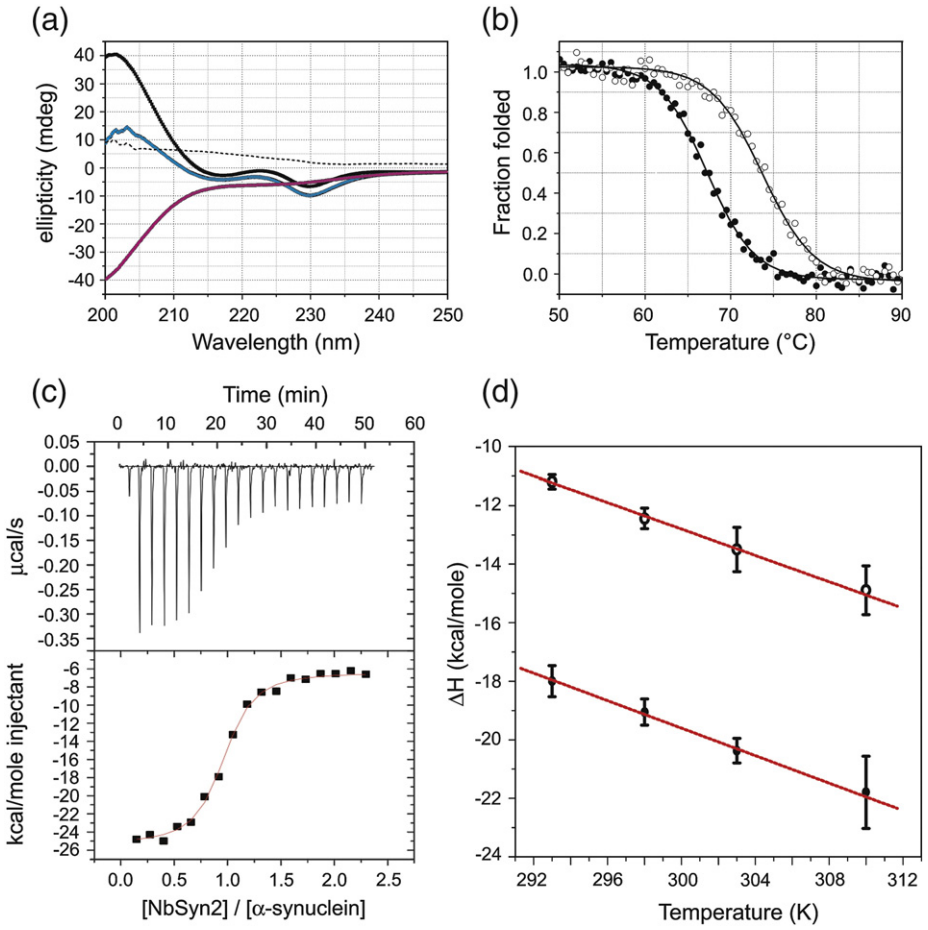

Fig. 1. CD and ITC measurements of the NbSyn2:α-synuclein interaction. (a) Far-UV CD spectra of NbSyn2 (black), α-synuclein (pink), and the α-synuclein:NbSyn2 complex (cyan) at 20 μM in 10 mM sodium phosphate buffer, pH 7.4, and 150 mM NaCl, at 25 °C. The difference spectrum (α-synuclein:NbSyn2 complex) − (NbSyn2 + α-synuclein) is shown as a broken line. (b) Fraction of folded NbSyn2 as a function of temperature during thermal denaturation and measured by CD at 222 nm, of the samples of NbSyn2 (●) and the 1:1 α-synuclein:NbSyn2 complex (○) at 20 μM in 10 mM sodium phosphate buffer, pH 7.4, and 150 mM NaCl. (c) ITC data for NbSyn2 at 25 °C in PBS buffer (traces are of similar quality for all experiments) (d) ΔH as a function of temperature for the α-synuclein:NbSyn2 complex (●) interaction and for the peptide N-YEPEA-C interacting with NbSyn2 (○). The slope of a regression line was used to define the ΔC_p of the interaction.

Table 1. Thermodynamic parameters of the NbSyn2:α-synuclein interaction as measured by ITC

Ligand	T (K)	ΔH (kcal mol^{-1})	$T\Delta S$ (kcal mol^{-1})	ΔG (kcal mol^{-1})	Stoichiometry	K_d (nM)	ΔC_p (kcal mol^{-1} K^{-1})[a]
Peptide[b]	293.1	−11.20±0.24	2.31±0.25	−8.88±0.07	0.98±0.01	240±26	−0.22±0.01
	298.1	−12.44±0.35	3.28±0.36	−9.16±0.09	0.99±0.01	190±30	
	303.1	−13.50±0.76	4.72±0.77	−8.78±0.14	0.94±0.02	460±110	
	310.1	−14.89±0.83	6.29±0.84	−8.61±0.09	0.92±0.03	850±130	
Full-length α-synuclein	293.1	−18.00±0.53	8.65±0.55	−9.35±0.12	0.99±0.01	106±21	−0.23±0.01
	298.1	−19.05±0.45	9.67±0.46	−9.39±0.10	0.93±0.01	130±23	
	303.1	−20.32±0.42	10.61±0.43	−9.71±0.10	0.87±0.01	99±17	
	310.1	−21.79±1.23	12.47±1.24	−9.33±0.16	0.91±0.03	260±69	

[a] The contribution of protonation to the value of ΔH was determined using 10 mM Tris–HCl buffer and 100 mM NaCl at pH 7.4 and was found to be insignificant.
[b] The sequence of the peptide, N-YEPEA-C, corresponds to residues Tyr136-Ala140 of full-length α-synuclein.

pH 7 as shown in Fig. 1b, while in the presence of α-synuclein, the T_m increases to 74±1 °C (Fig. 1b), showing that binding stabilizes NbSyn2 by 7±1 °C.

Thermodynamic parameters of the NbSyn2:α-synuclein interaction using isothermal calorimetry

Isothermal titration calorimetry (ITC) was also used to monitor the binding of NbSyn2 to α-synuclein (Fig. 1c). Measurements were performed at temperatures between 20 and 37 °C, and the data are consistent with a 1:1 bimolecular association between NbSyn2 and α-synuclein in each case, with K_d values of 106±21 , 130±23 , 99±17 , and 260 ±69 nM at 20 , 25 , 30 , and 37 °C, respectively (Table 1). These K_d values are typical of those measured for other *in vivo* matured camelid heavy-chain antibodies interacting with their ligands.[24]

The enthalpy, ΔH, and entropy, $T\Delta S$, contributions to the changes in Gibbs free energy, ΔG, associated with the binding of the two systems for every temperature and the values are summarized in Table 1. From the temperature dependence of the change in interaction enthalpy, we can deduce the change in heat capacity (ΔC_p) associated with the formation (Fig. 1d) of the complex between α-synuclein and NbSyn2. The value for ΔC_p of 0.23± 0.01 kcal mol^{-1} K^{-1} is typical of protein–protein interactions[49] and is largely attributable to the total change in solvent-accessible surface area (ASA) upon complex formation but may also include contributions from changes in conformations of either or both components.[50]

We performed identical ITC measurements using NbSyn2 and a peptide fragment of α-synuclein, encompassing the residues Y136-A140 of α-synuclein, which was found to be the epitope of NbSyn2 on α-synuclein (see below). We found that the corresponding affinity and ΔC_p value are very similar to those for the interaction with full-length α-synuclein (Table 1). This finding reveals that ΔC_p arises overwhelmingly from the direct binding of NbSyn2 to the residues located within the epitope of α-synuclein and not as a consequence of significant conformational changes within the remainder of the molecule.

NMR mapping of the NbSyn2 epitope

We used ^{15}N–^{1}H heteronuclear single quantum coherence (HSQC) spectroscopy to map the epitope of NbSyn2 on α-synuclein by observing perturbations to the backbone amide resonances. Titration of unlabeled NbSyn2 into ^{15}N-labeled α-synuclein resulted in both broadening and shifts of specific resonances in the HSQC spectrum of the latter. The resonances primarily affected are those corresponding to residues 130–140 (Fig. 2a and c), although small chemical shift (≤0.05 ppm) and intensity changes (≤50%) were also observed for residues adjacent to the C-terminal region at concentrations of NbSyn2 equivalent to that of α-synuclein. These latter effects indicate the existence of weaker binding interactions of this region; indeed, addition of NbSyn2 above equimolar concentrations relative to α-synuclein reveals the presence of a second binding site for the antibody fragment in α-synuclein, as a set of resonances (residues 110–129) shifts continuously and proportionately to the antibody concentration under these conditions. This second binding site is, however, of low affinity, with an estimated $K_d \geq 1$ mM compared to the $K_d \approx 100$ nM for the primary site, and is likely to be nonspecific. Moreover, binding at this second site is very sensitive to ionic strength but not to the sequence, as binding to NbSyn2 is also observed for β-synuclein, which has only 30% identity with α-synuclein in this region of the sequence[41] (data not shown).

Binding dynamics (observed as exchange rates in NMR experiments) have a strong influence on the line widths of NMR signals, and the extent of broadening depends strongly on the relative difference in resonant frequency between the bound and the free state of the protein (i.e., on the difference in chemical shifts) and on the rate of exchange between the two states. Slow- and fast-

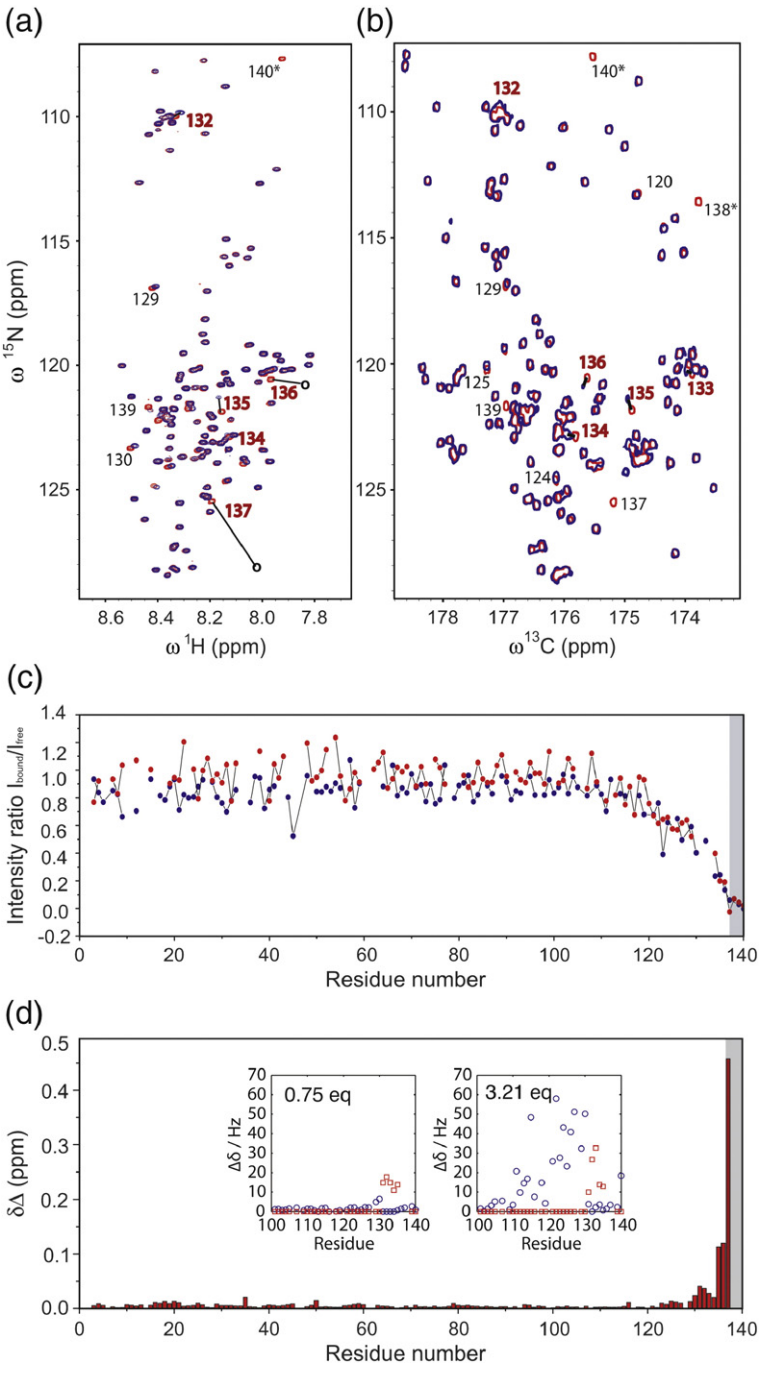

Fig. 2. (a) ^{15}N–^{1}H HSQC spectra of uniformly ^{15}N-labeled α-synuclein, free (red), and following the addition of 1 equivalent of unlabeled NbSyn2 (blue). The residues whose resonances are most strongly perturbed by antibody binding (i.e., showing a significant loss of intensity and/or a change in chemical shift of ≥0.02 ppm) are indicated. Resonances in the bound spectrum that are shifted significantly relative to their position in the unbound form are linked by a black line and the residue number is shown in red. (b) CON spectra of uniformly ^{13}C–^{15}N-labeled free α-synuclein (red) and following addition of 1 equivalent of unlabeled NbSyn2 (blue). Again, the residues whose resonances are most affected by the presence of NbSyn2 are indicated in red, and black lines connect corresponding resonances in the bound and unbound state. Asterisks indicate those residues that have been folded into the spectrum as a consequence of the limited spectral width. (c) Intensity of the spectrum of bound compared to free α-synuclein (I_{bound}/I_{free}), HSQC (red), CON (blue). In (c) and (d), a gray shaded area is added to the plot to indicate the residues in α-synuclein for which the resonance (and hence the chemical shift) of the bound state is unobservable. (d) Chemical shift changes in the free and bound states (change in chemical shift is defined as $[0.04\times(\delta^{15}N_{free}-\delta^{15}N_{bound})^2+(\delta^{1}H_{free}-\delta^{1}H_{bound})^2]^{1/2}$.[40]

exchange conditions result in, respectively, two distinct sharp peaks in the spectrum or a single sharp peak at a position between the bound and free chemical shifts, weighted by the molar fractions of the bound and the free molecules. Intermediate exchange regimes are characterized by different levels of line broadening.[51] By analysis of the resonances of α-synuclein that are shifted and broadened on binding NbSyn2, we can estimate that the exchange rate lies between 1 and 20 s^{-1} for the first binding site and is above 60 s^{-1} for the second binding site (Fig. 2d, inset).

No significant changes in intensities and shifts were observed for residues other than those discussed above. As a result of the spectral overlap in the HSQC spectra, however, several regions are difficult to analyze. To increase the dispersion within the spectra, we performed CON measurements[52] with and without different concentrations of added NbSyn2. The CON experiment correlates the ^{13}C

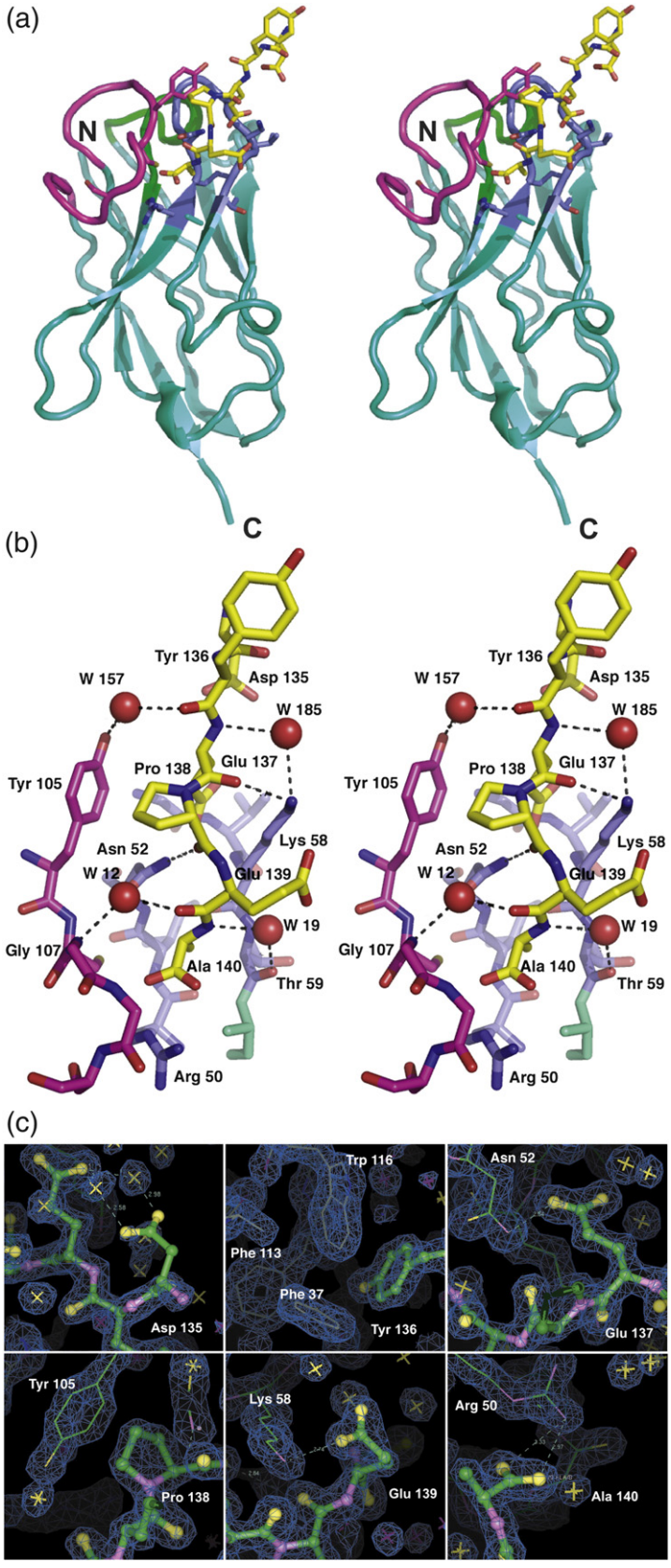

Fig. 3. (a) Stereo view of the crystal structure of NbSyn2 complexed with a synthetic peptide N-GYQDYEPEA-C. N- and C-termini are indicated for NbSyn2. The framework regions of the NbSyn2 structure are shown in cyan, and the atoms of the hypervariable loops are color coded: O, red; N, blue; S, yellow. The carbon atoms, C, are color coded differently for each loop to distinguish the CDR loops: green, CDR1; light blue, CDR2; magenta, CDR3. The peptide is shown in a ball-and-stick representation and atoms are color coded: C, yellow; O, red; N, blue. The side chains of the residues of NbSyn2 that have atoms within 5 Å of the peptide are represented as sticks. (b) Close-up stereo view of the peptide in the NbSyn2 binding site. Residues are color coded as in (a). Water molecules in the interface between the peptide and NbSyn2 are represented as red spheres. Peptide residues are labeled from Asp135 to Ala140. Residues in contact with main-chain atoms of the peptide or with water molecules bridging main-chain atoms of the peptide with atoms of NbSyn2 are labeled and hydrogen bonds are represented as black dotted lines. (c) Detailed view of the side-chain interactions between the residues of the peptide and those of NbSyn2. Residues of the peptide are represented as sticks, and those of NbSyn2 are drawn as lines. Atoms are color coded: C, green; N, pink; O, yellow. A $2F_o - F_c$ map contoured at 1 σ, is represented as a light blue mesh. The interactions for each side-chain are represented in different panels (from left to right, top panels: Asp135, Tyr136, and Glu137; bottom panels: Pro138, Glu139 and Ala140). Note that the side chain of Tyr136 interacts with residues of a symmetry-related NbSyn2 molecule.

carbonyl chemical shift of residue n with the ^{15}N chemical shift of residue $n+1$ and therefore results in a cross-peak in a ^{13}C–^{15}N 2D spectrum. The resonances that are observed to be broadened, as well as the extent of broadening, are essentially identical in the HSQC and CON spectra (Fig. 2a–c). In addition, the resonances of the residues that shift in the HSQC titrations are also observed to be shifted in the CON spectra.

Crystal structure of the NbSyn2–peptide complex

We have been able to gain insight into the atomic details of the NbSyn2:α-synuclein interaction by crystallizing and solving the x-ray structure of NbSyn2 complexed with the peptide N-GYQDYEPEA-C; the latter corresponds to residues 132–140 of α-synuclein and includes those identified by NMR as part of the epitope (Fig. 3). In the structure, we observe significant electron density only for the last six residues of the peptide; the other residues are therefore highly flexible or disordered, implying that they are not involved in specific interactions with NbSyn2. The residue Asp135 has the least well-defined electron density of these last six residues (Fig. 3c, first top panel), and although there is clear density for Tyr136, this residue is involved in crystal packing contacts with a symmetry-related complex (Fig. 3c, second top panel), implying that the conformation of the side chain of this residue could well differ from that found in solution.

Detailed analysis of the crystal structure reveals that the peptide binds to NbSyn2 in a pocket formed by residues of the complementarity-determining region (CDR)3 and CDR2 loops of the nanobody that make contacts with residues Tyr136, Glu137, Pro138, Glu139, and Ala140 of α-synuclein. The binding is primarily mediated through side-chain interactions and is mainly electrostatic in nature, although an important hydrophobic interaction occurs between Pro138 of the peptide and Tyr105 of NbSyn2, where the C^{γ} and C^{δ} positions in the cyclic aliphatic ring of Pro138 stack perpendicularly against the aromatic ring of Tyr105. In addition, although the C^{β} of Ala140 is deeply buried in a pocket formed between the CDR3 and CDR2 loops of the nanobody (Fig. 3b), the carbonyl groups of this C-terminal residue make a salt bridge with Arg50 of NbSyn2 (Fig. 3c). The peptide main-chain atoms, apart from the carbonyl groups of Ala140 and the carbonyl oxygens of Glu137 and Pro138, which make direct hydrogen bonds with residues of NbSyn2, either are exposed to solvent or make indirect contact with the nanobody through bridging water molecules (Fig. 3b).

The total change in ASA (ΔASA) upon formation of the complex is 569.1 Å^2 (237.9 Å^2 of the NbSyn2 and 331.2 Å^2 of the peptide). The fraction of this value that is nonpolar is 318.0 Å^2, (143.1 Å^2 of NbSyn2 and 174.9 Å^2 of the peptide). Based on the parameterization data of Murphy and Freire,[53] this amount of buried surface area leads to a calculated ΔC_p of binding of 0.08 kcal mol^{-1} K^{-1}. This value represents only a fraction, approximately 30%, of the ΔC_p measured using our ITC experiments (see above) and therefore suggests that the additional change in heat capacity originates from structural rearrangements within the NbSyn2 molecule.

Binding of α-synuclein to ^{15}N-labeled NbSyn2

We used solution-state NMR spectroscopy to characterize further the binding of α-synuclein to NbSyn2 and to investigate the structural changes that occur in the NbSyn2 molecule binding to either full-length α-synuclein or a peptide that includes residues of α-synuclein in the binding region. The HSQC NMR spectra have been assigned previously by conventional 3D methods on uniformly ^{13}C–^{15}N-labeled NbSyn2 at pH 4.8.[54] In order to be able to translate these assignments to the spectra recorded under the conditions used in the titrations described above, we monitored the perturbations to the resonances of the residues of NbSyn2 as the pH was shifted from 4.8 to 7.4 at 298 K; the resonances originating from the six histidines at the C-terminal end of the NbSyn2 (the so called His-tag) are severely broadened at high pH, as are residues Gly26, Trp36 (CDR1), Gly55-Gly56, Asp63-Ser64 (CDR2), and Tyr107-Gly117 (CDR3). This phenomenon could be a consequence of a higher solvent exchange rate at this pH or of the fact that these residues in the unbound state are in dynamic exchange between different conformations at a rate that is similar to the difference in chemical shifts between these conformations. Lowering the temperature restores the intensity of some of these resonances, but even at 283 K the resonances of residues Gly53, Val57, Lys58, and Thr59 of the CDR2 region and Gly104, Tyr105, and Cys106 of the CDR3 region remain unresolved.

Despite the fact that not all residues are visible in the NMR spectra of unbound NbSyn2, we investigated the changes that occur upon α-synuclein binding. Addition of α-synuclein causes large alterations in chemical shift values of the resonances of certain residues in the HSQC spectrum and the emergence of new peaks. Using a double-labeled sample of ^{13}C–^{15}N-NbSyn2 at pH 7.4 and 283 K, in the presence of 2 molar equivalents of α-synuclein, analysis of a triple-resonance HNCA experiment enable the identification and the assignment of the cross-peaks of every residue in the bound state of NbSyn2. The assigned signals included those from residues located in the CDR3 binding loop that are unobservable in the unbound state, suggesting that this region of the protein adopts a more clearly defined conformation in the bound state compared to the free protein.

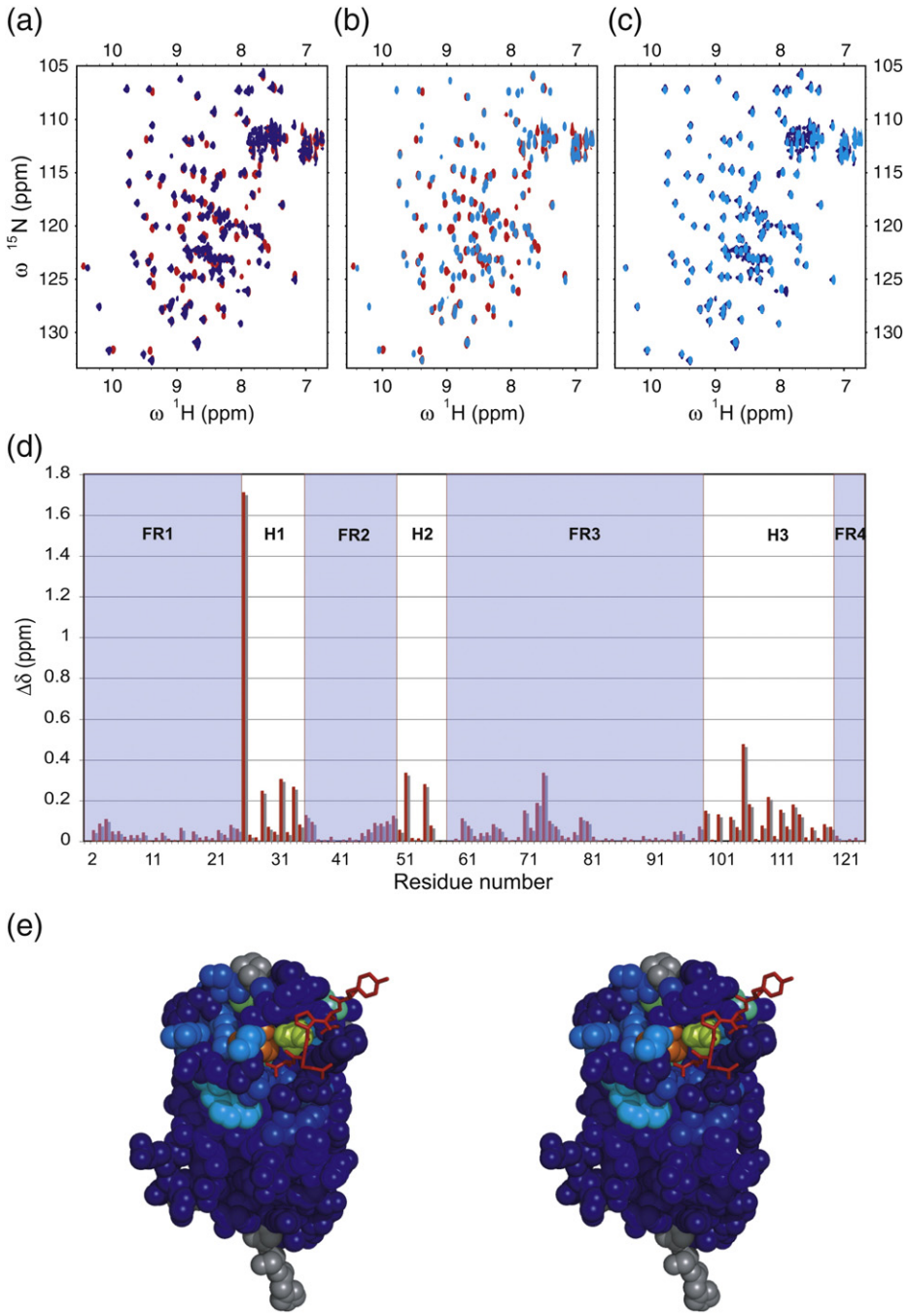

Fig. 4. (a) Overlay of the ^{15}N–^{1}H HSQC spectra of NbSyn2, free (red), after addition of two equivalents of full-length α-synuclein (blue) at 298 K. (b) Overlay of the ^{15}N–^{1}H HSQC spectra of NbSyn2 at 298 K, without (red) and with (light blue) two equivalents of a peptide encompassing the last 12 residues (Ser129-Ala140) of α-synuclein. (c) Overlay of the ^{15}N–^{1}H HSQC spectra of NbSyn2, after addition of two equivalents of the peptide Ser129-Ala140 (light blue) at 298 K and that of NbSyn2 at 298 K after addition of two equivalents of full-length α-synuclein (blue). (d) Chemical shift perturbations of NbSyn2 at 283 K upon binding to full-length α-synuclein. The regions corresponding to the immunoglobulin framework are shaded in light blue and indicated as FR1–4, and those corresponding to the antigen binding loop regions are indicated as H1–3. (e) Chemical shift perturbations from the spectra shown in (b) mapped on to the structure of NbSyn2 in complex with the peptide N-GYQDYEPEA-C determined in this work (see text); the magnitudes of the shifts of NbSyn2 residues are color coded going from dark blue (insignificant shift) to red (major shift). The residues for which no assignments are available are colored gray. The peptide is represented in stick format and colored red.

The residues for which the resonances show the most significant changes in chemical shift are located in the CDR regions (Fig. 4). For CDR1, the resonances involved are those of residues Gly26, Ser29, and Tyr32-G35, while in CDR2, the most notable effects of binding are observed for residues Asn52-Gly53 and Gly55-Val56. The resonances of residues Val57-Thr59 are also perturbed, as they show strong signals in the spectrum of NbSyn2 bound to α-synuclein, whereas in the non-liganded spectrum of NbSyn2, these resonances could not be detected. Hence, we were unable to determine the chemical shift perturbations for the resonances of these residues associated to the binding of α-synuclein to NbSyn2. In CDR3, a yet larger number of residues are perturbed than in the first two loops and include Gly104-Gly107, Ser109-Trp110, Asn112, Gly114, Gly117, and Gly119. To a lesser extent, several of the residues located in the framework regions of the immunoglobulin fold, such as Gly2-Gly10, Gln13, Gly16, Leu18, Cys22, Ala24, Arg45-Arg50, Tyr61-Arg68, Cys97, and Ala98, and those in the extended loop region from Ile71-Tyr81, also experience alterations in their chemical shifts as a result of the addition of α-synuclein.

To assess the detailed state of the binding of the nanobody to the epitope of α-synuclein independently of the rest of the protein, we designed a peptide, based on the epitope identified by NMR (see above), encompassing the last 12 residues of α-synuclein, and probed its binding to ^{15}N-labeled NbSyn2 in an HSQC titration experiment. The spectra of the antibody containing 1 molar equivalent of added peptide overlays exactly with the corresponding spectra of NbSyn2 bound to full-length α-synuclein. This result indicates that the binding is structurally similar in both cases and therefore essentially independent of the structural context of the epitope (Fig. 4c).

We then mapped the chemical shift perturbations induced by the binding of α-synuclein onto the structure of NbSyn2 (Fig. 4e), an analysis that shows that the resonances of the residues located in the peptide-binding pocket experience the largest shifts. The resonances of many other residues of NbSyn2, which are not in immediate contact with the peptide molecule, also shift significantly, however, and are indicative of conformational changes within the NbSyn2 molecule upon binding to the peptide. Most remarkable is the large shift of Gly26, the first residue of CDR1 and hence one that plays a pivotal role in the structure of the CDR1 loop in antibodies.[55] Such secondary shifts are largely those of residues in CDR1–3 and are therefore likely to indicate rearrangements of these loops induced by binding. This observation and the fact that the resonances of many residues of NbSyn2 become visible on binding to α-synuclein suggest that the loops become more highly ordered on binding through a cooperative network of interactions. Importantly, binding of α-synuclein leads to an increased thermal stability of NbSyn2 (Fig. 1b), and this change in dynamics might explain the difference between the calculated and measured ΔC_p value in the ITC experiments.

NbSyn2 binds to amyloid fibrils formed from α-synuclein

In the light of the observation that NbSyn2 binds to its epitope both in the form of a short peptide and when part of the full-length protein, we decided to explore whether or not the antibody fragment would recognize its epitope when the latter is present in the fibrillar state of α-synuclein. We therefore prepared a homogeneous sample of α-synuclein fibrils, and addition of 1 molar equivalent of α-synuclein, in this fibrillar form, to ^{15}N NbSyn2 resulted in an immediate and uniform decrease in the intensity of the HSQC spectrum of the latter (Fig. 5a and b); this intensity decreased further on the addition of 2 molar equivalents of fibrillar α-synuclein. Following addition of 4 molar equivalents of α-synuclein in its fibrillar state, we observed a complete loss of visible peaks in the ^{13}N–^{1}H spectrum of NbSyn2. These results are fully consistent with a model in which the NbSyn2 resonances become broader as a result of the slower tumbling of the nanobody when bound to the fibrils; the latter effect then gives rise to a fast transverse relaxation rate that increases proportionally with the molecular weight of the complex.[56] In the present case, this slower tumbling can be attributed to the binding of the NbSyn2 molecules to the large fibrillar particles. The associated broadening of the signals, however, is not simply proportional to the number of equivalents of α-synuclein molecules in the fibrils added to the NbSyn2 sample and indicates that there is a dynamic equilibrium between the free monomeric NbSyn2 and that bound to α-synuclein in the fibrils. The fact that multiple equivalents of molecules of α-synuclein in its fibrillar form are necessary to give rise to complete broadening of the spectrum indicates that only a fraction of the total number of C-terminal regions of α-synuclein is accessible to the antibody fragment; that is, the majority are sequestered within the fibrillar structure.

To explore further the binding of NbSyn2 to the fibrils, we performed immunogold labeling and transmission electron microscopy (TEM; Fig. 5c and d). In these experiments, we added NbSyn2 in solution to a sample of preformed α-synuclein fibrils and probed the location of the nanobodies (which are engineered to contain six histidines at the C-terminal end of the molecule to facilitate purification) using an anti-His-tag mouse monoclonal antibody and a secondary rabbit anti-mouse monoclonal antibody labeled with a 10-nm gold particle. Figure 5c clearly shows the gold particles as black dots located along the length of the fibrils in the

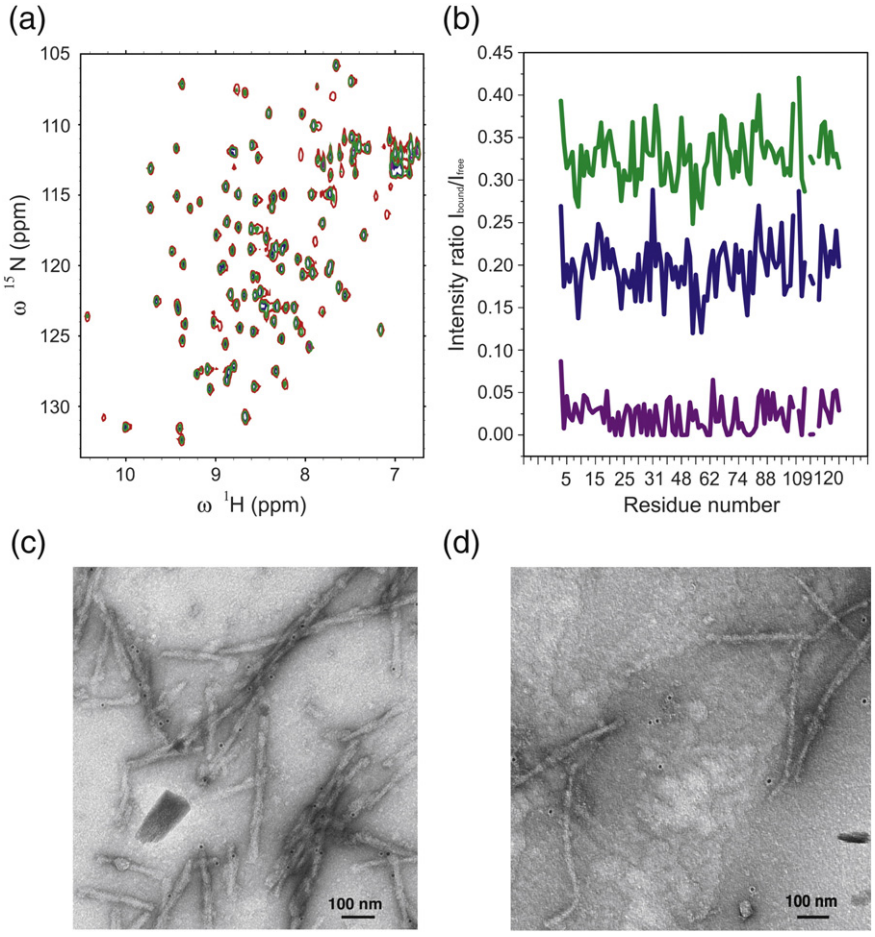

Fig. 5. NbSyn2 binding to α-synuclein fibrils. (a) ^{15}N–^{1}H HSQC spectra of NbSyn2, free (red), and following the addition of 1 (green), 2 (blue), and 4 (purple) molar equivalents of fibrillar α-synuclein. (b) The intensity of the respective ^{15}N–^{1}H HSQC spectra as a function of the sequence of NbSyn2. (c) TEM images of negatively stained α-synuclein fibrils co-incubated with NbSyn2 and anti-His-tag monoclonal antibodies conjugated to 10- nm gold particles (black dots). (d) Negative control in which NbSyn2 was omitted but all other steps were the same as in (c). The background and apparent amorphous material seen on the grids are non-specific effects attributable to the treatment of the grids as described in Materials and Methods.

electron microscopy (EM) images; these dots result from the fact that the mouse monoclonal antibody conjugated with gold label binds to the anti-His antibody in complex with the NbSyn2 antibody fragment bound to the fibril. Figure 5d represents the negative control where no NbSyn2 was added to the solution of the α-synuclein fibrils, and hence no gold labels attached to the fibrils are observed following treatment with the antibody molecules. Some gold particles are, however, visible, but are scattered randomly over the surface, indicating non-specific adsorption to the EM grid.

NbSyn2 does not significantly affect the conversion of α-synuclein into amyloid fibrils

As NbSyn2 binds to monomeric α-synuclein, we sought to investigate its effect on the aggregation properties of the protein. Figure 6a shows that the addition of a 1 molar equivalent of NbSyn2 to a 70-μM sample of α-synuclein in phosphate-buffered saline (PBS) buffer at 37 °C, under conditions of continuous stirring, only minimally perturbs the time course of the increase in the fluorescence of thioflavin T (ThT),[57] a dye that binds to amyloid fibrils; a slightly shorter lag phase is observed for the NbSyn:α-synuclein sample. In a parallel set of experiments, however, we monitored the time course of the change in the fluorescence of 1-anilino-8-naphthalene sulfonate (ANS),[58] a dye that binds to exposed hydrophobic patches on the surface of proteins (Fig. 6b). No significant differences for a series of solutions containing different ratios of NbSyn2 and α-synuclein were observed. In control experiments, NbSyn2 itself was shown not to aggregate under the conditions of these experiments.

This evidence therefore points to the conclusion that NbSyn2 does not significantly influence the

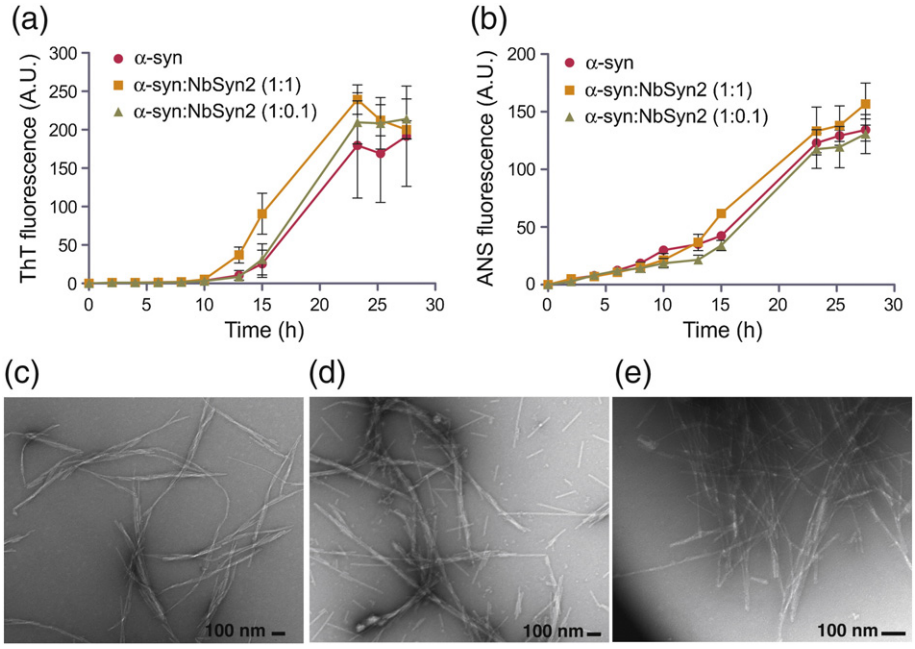

Fig. 6. Kinetics of aggregation of a-synuclein with or without NbSyn2, monitored by (a) ThT and (b) ANS binding assays. The nanobody was added at 1.0 (yellow squares) and 0.1 (green triangles) equivalents, and the fluorescence was sampled at various time points along the aggregation reaction. (c–e) TEM images of the reaction mixtures at the endpoint of the aggregation reactions after staining with uranyl acetate. (c) α-synuclein, (d) α-synuclein with 1.0 molar equivalent of NbSyn2 added, (e) α-synuclein with 0.1 molar equivalent of NbSyn2 added.

formation of amyloid fibrils by α-synuclein, even at a 1:1 stoichiometry, suggesting that it is not involved in any of the rate-limiting steps of the aggregation reaction under the conditions studied in this work, and that the binding process is highly dynamic. In support of these conclusions, TEM was used to image all the fibrils at the endpoint of the reaction and no significant differences in fibril morphology could be detected. However, in the samples containing an equimolar mixture of α-synuclein and NbSyn2, a higher number of shorter fibrils observed (Fig. 6d), suggesting a higher rate of fragmentation and therefore a shorter lag phase in the aggregation reaction probed by ThT fluorescence. These effects are perhaps attributable to a slightly lower degree of fibril maturation as a result of the binding of NbSyn2 to the fibrils, making them more prone to fragmentation and hence lead to a shorter lag-phase.

Discussion

The interaction of NbSyn2 and monomeric α-synuclein

We have obtained a camelid antibody, NbSyn2, through a strategy that involved immunization followed by phage display, recombinant expression in *Escherichia coli* and purification of the soluble nanobody. This nanobody binds with nanomolar affinity to the C-terminal region of full-length α-synuclein. From ITC measurements as well as from CD and NMR spectroscopy, we have found that this tight binding has a 1:1 stoichiometry and does not induce large changes in secondary or tertiary structure of either protein. ITC can detect conformational movements by evaluating the change of the value of the heat capacity, ΔC_p, on binding;[49,50] the ΔC_p values are indistinguishable for NbSyn2 binding to both full-length α-synuclein and peptide fragments encompassing the epitope. The observed ΔC_p for the NbSyn2:α-synuclein interaction, therefore, corresponds to the value calculated for the burial of the α-synuclein epitope resulting from binding to NbSyn2, without any significant contributions from additional structural changes within the α-synuclein molecule itself.

NMR studies of ^{15}N-labeled α-synuclein using HSQC spectroscopy do not reveal any major changes in chemical shift or signal intensity associated with the binding of NbSyn2 other than that of the residues in the binding region. Previous studies of the interaction of polyamines with α-synuclein have revealed significant changes in the intensities of resonances in the HSQC spectrum corresponding to residues at the N-terminal region of the protein.[17] These changes suggest that binding causes a disruption of weak but detectable contacts between residues at the C-terminus and in the NAC region and N-terminus of the protein. The absence of similar

intensity changes in the α-synuclein NMR spectrum in the presence of NbSyn2 indicates that the conformational ensemble of α-synuclein is essentially unchanged on binding to the nanobody. This conclusion is supported by preliminary paramagnetic relaxation enhancement measurements[43] (A. Vuchelen, personal communication) on NbSyn2 bound to spin-labeled ^{15}N α-synuclein, showing that the long-range interactions that are present in more compact members of the conformational ensemble of the protein are preserved. This lack of conformational perturbation is consistent with the fact that the antibody fragment does not influence significantly the *in vitro* aggregation properties of α-synuclein.

To analyze the interaction between α-synuclein and NbSyn2 at atomic resolution, we crystallized and solved the X-ray structure of NbSyn2 in complex with the peptide N-GYQDYEPEA-C, encompassing residues 132–140 of α-synuclein. The structure revealed that there is measurable density only for the last six residues (DYEPEA) of the peptide, and that the last four residues (EPEA) are clearly anchored between CDR2 and CDR3 of NbSyn2. The absence of electron density for the remaining residues shows that these do not interact specifically with NbSyn2 and are therefore disordered in the crystal structure. The structure shows further that the residues of α-synuclein that interact with NbSyn2 are bound in an extended conformation and that the interaction is primarily mediated by side-chain interactions, a feature that is commonly found in antibody–peptide complexes.[59]

Comparison of the crystal structure and the NMR data reveal interesting features of the interaction between NbSyn2 and α-synuclein. Indeed, detailed examination of the NMR data for ^{15}N α-synuclein containing a 1 molar equivalent concentration of NbSyn2 shows that the extent of line broadening of the amide (in ^{15}N–^{1}H HSQC measurements) and carbonyl (in ^{13}C–^{1}H CON measurements) resonances of residues 130–140 gradually increases along the sequence of the C-terminal region; for residues Pro138, Glu139, and Ala140, the extent of broadening is so large that the resonances of the corresponding residues become undetectable. This trend is accompanied by an increased difference in chemical shifts for the resonances of the bound and free states of residues 130–140 of α-synuclein towards the C-terminus. In the crystal structure, no electron density is observed for residues Gly132, Tyr133, and Gln134, indicating that they remain disordered in the bound complex and are not involved in contacts with NbSyn2. In addition, residues Asp135, Tyr136, and Glu137, which are observable in the crystal structure and which are located at the periphery of the binding site, also have resonances that shift towards a new position in the ^{15}N–^{1}H HSQC spectrum, with that of the strongly interacting Glu137 having the largest shift. Taken together, these results indicate that there are only minor perturbations in the chemical environment of α-synuclein in the region 130–136 associated with the binding of the nanobody.

The fact that most of the residues of α-synuclein that are involved in direct contact with residues of the nanobody are broadened beyond detection in the HSQC and CON spectra of the complex is intriguing and suggests that these residues are involved in dynamic events that are in the intermediate exchange regime in the NMR spectrum, that is, are taking place on the approximately millisecond timescale. The variation in magnitude of NMR chemical shift changes between the bound and unbound state, along with the nanomolar binding affinity, indicates, however, that this broadening is unlikely to result simply from the exchange between the bound and the unbound states of α-synuclein. The crystal structure of the NbSyn2–peptide complex reveals, however, that the interaction between the two molecules is mediated primarily by side-chain contacts. Only a few direct contacts are made with backbone atoms of the peptide (similarly with the full-length α-synuclein molecule) and most of the amide and carbonyl residues located in the binding regions make indirect contacts through bridging water molecules. This observation suggests that broadening of the amide and carbonyl resonances of the residues of α-synuclein involved in binding could be a consequence of the dynamics of the interactions that result from the residence times of these bridging water molecules involved in the binding interactions. This strong involvement of water molecules in the complex between NbSyn2 and α-synuclein suggests further that solvent molecules could be of considerable importance more generally in the intra- and intermolecular interactions of α-synuclein and indeed of other IDPs whose residues in their soluble states are virtually always in intimate contact with solvent water.

The CD data show that NbSyn2 gains thermal stability upon binding to α-synuclein, and the NMR line width data indicate that the interacting region of NbSyn2 becomes significantly more ordered. This latter phenomenon might also be a general feature of proteins binding to intrinsically unstructured sequences, as similar effects have been noted in several complexes formed between other unstructured proteins and molecular chaperones.[60–62] Moreover, the calculated ΔC_p for the NbSyn2:α-synuclein complex, based on the surface area burial from the crystal structure, is only approximately 30% of the measured ΔC_p obtained from ITC experiments. Although this calculated value is only an estimate, it is consistent with the hypothesis that additional contributions to ΔC_p are likely to exist and can be attributed to conformational changes, either through perturbations in the extent of exposed hydrophobic surface area as a result of CDR loop rearrangements

or through the enhancement of hydrogen-bonding networks[63] within the complex.

NbSyn2 as a structural probe of the different aggregation states of α-synuclein

The present findings reveal that NbSyn2 binds specifically to the C-terminus of α-synuclein and that it does not significantly perturb either the characteristics of the conformational ensemble of the soluble form of the protein or its aggregation into fibrillar amyloid species. Using X-ray crystallography, NMR spectroscopy and immunogold labeling, we have established that NbSyn2 binds to its epitope on α-synuclein in very different structural contexts. Specifically, we show that the antibody can bind to the fibrillar form of α-synuclein, unequivocally confirming that in at least a significant fraction of the molecules in the fibrils, residues 130–140 are located outside the fibrillar core and are sufficiently accessible to solvent to allow the interaction with other molecular species. These data are consistent with a variety of studies that indicate that the C-terminal region of α-synuclein is located on the surface of the fibrils and has extensive motional freedom.[64,65] Our data suggest, however, that in the fibril, only one α-synuclein in four is able to bind tightly to NbSyn2 and indicates either that not all C-termini in the fibril are accessible or that binding of the NbSyn2 generates sufficient local steric hindrance to inhibit the interaction of nanobodies with adjacent epitopes.

A recent solid-state NMR study suggests that the structure of α-synuclein in a protofibril involves a five-stranded β-sheet, with the C- and N-termini located on different sides of the protofibril.[64] In addition, it has been proposed that four protofilaments make up the mature fibril,[64,65] a finding that is interesting in the context of our observation that NbSyn2 molecules bind to one in four α-synuclein molecules in the fibrillar state. It seems likely that when the protofilaments intertwine to form mature fibrils in the majority of the molecules, the C-terminal residues are inaccessible at least to a soluble protein such as NbSyn2. Taken together, these results indicate that the recognition of the C-terminal region of α-synuclein by NbSyn2 can be used to probe the exposure of the C-terminal region of α-synuclein under different conditions, as well as of aggregated species formed along the fibril formation pathway and in the maturation of α-synuclein fibrils over time. In addition, possible steric restrictions to the binding of adjacent epitopes of NbSyn2 within the aggregated species can also provide information on the spatial arrangement of the α-synuclein monomers within these species.

Finally, the fact that the antibody fragment does not impose major structural rearrangements within the conformational ensemble of the α-synuclein monomer is highly beneficial in the context of probing its molecular environment in other states. Indeed, the results of the studies described here suggest that NbSyn2 should be an extremely valuable probe of different species populated during the process of fibril formation. The finding that NbSyn2 has no major influence on the aggregation kinetics of α-synuclein, for example, suggests that the C-terminal region plays no part in the structure or stability of any intermediate species whose formation affects the aggregation kinetics. Furthermore, these data suggest that NbSyn2 has the potential to be an excellent, structurally silent reporter to probe the aggregation process of α-synuclein under different conditions, including the events occurring *in vivo*, and indeed to define the interactions of this protein with other molecular species, most interestingly to explore its functional role in living systems.

Materials and Methods

All chemicals and reagents were purchased from Sigma-Aldrich, Dorset, UK, unless otherwise stated. All protein concentrations were measured by UV absorbance spectroscopy using molecular extinction coefficient, which was calculated based on the sequence of the proteins, at 280 nm of 5960 M^{-1} cm^{-1} for α-synuclein and 27,180 M^{-1} cm^{-1} for NbSyn2.

Isolation, expression, and purification of NbSyn2 and α-synuclein

The camelid antibody NbSyn2 was isolated from a dromedary immunized with α-synuclein and then selected by phage display, essentially according to published protocols.[66,67] In short, the immunization was boosted at several intervals during a six-week period. Lymphocytes were isolated and a VHH phage display library was constructed. *In vitro* selection on α-synuclein resulted in the isolation of one family of binders: NbSyn1a,b,c. A new selection in the presence of NbSyn1a and after three rounds of panning allowed the isolation of NbSyn2. NbSyn2 was subsequently sequenced and recloned in a modified pHEN vector (pHEN6[67]) containing a sequence coding for six consecutive histidines at the C-terminus of the nanobody. NbSyn2 was then expressed in the periplasm of *E. coli* and purified using immobilized metal affinity chromatography and size-exclusion chromatography essentially according to published protocols.[67]

Expression and purification of ^{14}N, ^{15}N, and $^{15}N,^{13}C$ α-synuclein[68] and ^{15}N and $^{15}N,^{13}C$ NbSyn2[54] for NMR measurements were carried out according to published protocols.[54,68]

CD measurements

Three samples, (1) α-synuclein, (2) NbSyn2, and (3) an equimolar mixture of α-synuclein and NbSyn2, were prepared at identical molar concentrations (20 μM in

10 mM phosphate buffer, pH 7.4, and 150 mM NaCl) originating from concentrated stock solutions of α-synuclein and NbSyn2, using high-precision Hamilton syringes for volumetric measurements. CD measurements were performed on a Jasco J-810 spectrometer using a cuvette of 0. 1 cm path length containing protein at a concentration of 20 μM in 10 mM phosphate buffer, pH 7.4, and 150 mM NaCl. Spectra were recorded between 250 and 200 nm at 25 °C. Twenty scans were averaged without smoothing and corrected for the spectra of the buffer. To monitor the secondary-structure perturbations that occur upon formation of the NbSyn2:α-synuclein complex, both spectra of the free α-synuclein and the free NbSyn2 were subtracted from the spectrum of the NbSyn2:α-synuclein sample. Thermal unfolding of the antibody fragment was followed by measuring the CD signal at 220 nm in 10 mM phosphate buffer at pH 7.4 and 150 mM NaCl. The temperature was increased monotonically in the range from 20 to 90 °C, at a rate of 0.5 °C min^{-1}. Data were acquired with a reading frequency of 20 s^{-1}, a 1-s integration time, and a 2-nm bandwidth.

Isothermal calorimetry measurements

Calorimetric measurements were recorded using an iTC200 calorimeter (MicroCal, LLC, Northampton, MA, USA). A solution of 40 μl NbSyn2, at a concentration of 75 μM, was titrated in aliquots of 2 μl into the calorimetric cell, containing 203 μl of 5 μM α-synuclein. Both proteins were dialyzed prior to measurements in exactly the same buffer containing 10 mM phosphate and 150 mM sodium chloride at a pH of 7.4. Each injection was performed every 150 s at the desired temperature. A titration of NbSyn2 in the sample cell containing only buffer was subtracted from the actual binding experiment before analysis. The thermodynamic analysis was performed using the Microcal analysis software (Origin 7.0) with a 1:1 binding model. The temperature dependence of ΔH allowed the calculation of ΔC_p through the relationship $\Delta C_p = \delta \Delta H / \delta T$. The contribution of protonation to ΔH was evaluated using a 10-mM Tris–HCl buffer and 100 mM NaCl at pH 7.4.

Aggregation measurements

Samples of 70 μM α-synuclein or NbSyn2, or a mixture of the two proteins, were incubated in 10 mM phosphate buffer, pH 7.4, and 150 mM NaCl at 37 °C under continuous stirring with a magnetic stir bar. Aliquots (5 μl) were removed at various time points, and ThT was added in 10 mM phosphate buffer, pH 7.4, and 150 mM NaCl to give a final concentration of 2 μM. ThT fluorescence was measured using a Cary Eclipse fluorimeter (Varian). Identical samples were also used to monitor ANS binding. Samples at the end of the reaction were analyzed on SDS-PAGE and imaged by negative staining using uranyl acetate and TEM (20,000–80 ,000× magnifications at 80 kV excitation voltages using a Philips CM100 transmission electron microscope).

Crystallization of the NbSyn2–peptide complex

Crystallization of the NbSyn2 complexed with a synthetic peptide (sequence NH_2-GYQDYEPEA-COOH) (BIO-SYNTHESIS, INC., Texas, USA) was achieved using a crystallization robot Phoenix (Art Robbins Instruments, Sunnyvale, CA) and a sitting drop vapor diffusion assay. One hundred thirty-three microliters of 10 mg/ml of NbSyn2 was first mixed with 15 μl of peptide (at 20 mg/ml) before dispensing in a JB Classic 1–4 (G10) screen (Jena Biosciences, Jena, Germany). Drops (100 nl) were mixed with 100 nl of the precipitant solution. Crystals were obtained under the following conditions: 25% w/v polyethylene glycol (PEG) 6000, 100 mM Hepes, pH 7.5, and 100 mM LiCl were subsequently harvested and transferred in a cryo-protectant solution (25% w/v PEG 6000, 100 mM Hepes, pH 7.5, and 100 mM LiCl and 10% PEG 400) and flash-frozen in liquid nitrogen for data collection.

Data collection and structure solution

Diffraction patterns for frozen crystals of the NbSyn2–peptide complex were obtained at the X11 beamline equipped with a MAR555 detector, at the European Molecular Biology Laboratory using the Deutsches Elektronen-Synchrotron (Hamburg, Germany). Data were processed using Mosflm,[69] and Pointless and Scala[70] were used to determine the space group and scale and merge the data, respectively. Molecular replacement using the program Phaser[71] and a model for NbSyn2, namely, Protein Data Bank entry 1HCV,[72] was used to obtain the phase information associated with the structure factors. Model building and refinement were achieved using the programs ARP/wARP[73] and Refmac5[74] as implemented in the CCP4 suite.[74] The graphics program Coot[75] was used to interpret the electron density maps and for refinement of the model. Data collection and refinement statistics are listed in Table 2. The change in ASA upon the formation of the NbSyn2:α-synuclein complex was calculated using the web-based server ProtorP.[76] Figures were prepared using the program PyMOL‡.

NMR spectroscopy

All NMR experiments were performed using Bruker Avance 500 - or 700-MHz spectrometers equipped with cryo-probes. All NMR data were subsequently processed using NMRpipe[77] and the program SPARKY[78] was used for analysis of the data.

^{15}N–^{1}H HSQC measurements of labeled α-synuclein with or without ^{14}N NbSyn2

Standard ^{15}N–^{1}H HSQC experiments were carried out at a ^{1}H frequency of 700 MHz. Spectra of ^{15}N-labeled α-synuclein were recorded at different molar equivalents of unlabeled NbSyn2 (0.25, 0.5, 0.75, 1.0, 1.25, 1.5, 1.75, 2.0, 2.5, 3.0, and 3.25) by titration of small volumes of a concentrated stock solution of NbSyn2. All experiments were recorded in 10 mM phosphate buffer, pH 7.4, and at 283 K.

‡ www.pymol.org

Table 2. Data collection and refinement statistics (molecular replacement)

	NbSyn2:α-synuclein
Data collection	
Space group	$C222_1$
Cell dimensions	
a, *b*, *c* (Å)	60.17, 63.12, 62.87
α, β, γ (°)	90.00, 90.00, 90.00
Resolution (Å)	1.62 (1.62)
R_{sym} or R_{merge}	11.5 (54)
$I/\sigma I$	23.3 (4.3)
Completeness (%)	99.93 (99.9)
Redundancy	14.3 (14.2)
Refinement	
Resolution range (Å)	30–1.62 (1.71–1.62)
No. of reflections	14,361
R_{work}/R_{free}	15.63/20.26
B-factors (Å^2)	
Protein	15.8
Peptide	22.3
Water	26.6
r.m.s.d.	
Bond lengths (Å)	0.018
Bond angles (°)	1.693

The values in parentheses represent those of the highest-resolution shell.

Assignment of the ^{15}N–^{1}H HSQC spectra of labeled α-synuclein bound to ^{14}N NbSyn2

The amide resonances and C^{α} and C^{β} chemical shifts were determined previously[43,46] and used in the further analysis of the data. The chemical shifts of the α-synuclein resonances in its complex with NbSyn2 were assigned using a series of standard 3D experiments: CBCA(CO)NH and HNCACB. Sample integrity checks were performed between and after each 3D experiment by recording ^{15}N–^{1}H HSQC spectra.

^{13}C–^{15}N CON measurements of ^{15}N,^{13}C-labeled α-synuclein with or without ^{14}N NbSyn2

^{13}C–^{15}N CON experiments, which correlate the ^{13}C carbonyl chemical shift of residue *n* with the ^{15}N chemical shift of residue *n*+1, were performed as described previously.[52] The assignments of all cross-peaks in the spectra were obtained from Bermel *et al.*[52] and carried out at a ^{1}H frequency of 500 MHz. In total, two CON spectra were recorded for ^{15}N,^{13}C-labeled α-synuclein free and after addition of 1 equivalent of ^{14}N NbSyn2. The spectra were recorded on a 500-MHz Bruker Avance spectrometer equipped with a cryo-probe. The sample buffer was 10 mM phosphate buffer at pH 7.4 and the temperature was set at 283 K. The assignments of the CON cross-peaks of α-synuclein in the bound form were obtained by comparing the ^{15}N chemical shifts for the corresponding peaks in the assigned ^{15}N–^{1}H HSQC spectrum for bound α-synuclein.

^{15}N–^{1}H HSQC measurements ^{15}N NbSyn2

Titrations of full-length ^{14}N α-synuclein and a ^{14}N 12-residue peptide, N-SEEGYQDYEPEA-C (Genemed Synthesis Inc., New York, USA), were carried out with ^{15}N-labeled NbSyn2 at 0.3 mM in 20 mM phosphate buffer, pH 7.4, at 298 and 283 K.

Assignment of ^{15}N,^{13}C-labeled NbSyn2 bound to full-length α-synuclein and a peptide fragment of α-synuclein

We have reported the assignments of the backbone resonances of NbSyn2, at pH 4.8 and at 298 K, elsewhere.[54] The backbone assignments of samples of ^{15}N,^{13}C-labeled NbSyn2 at 0.3 mM in 20 mM phosphate buffer at pH 7.4 bound to α-synuclein were obtained by means of HNCA experiments at a ^{1}H frequency of 500 MHz.

Preparation of α-synuclein fibrils

α-Synuclein fibrils were prepared in two steps. Fibrils were initially prepared by vigorous agitation of 70 μM α-synuclein in PBS (10 mM phosphate, pH 7.5, 100 mM NaCl, and 0.1% NaN_3) for 48 h at 37 C. The solution was centrifuged (30 min, 16,000***g***), the supernatant was discarded, and the fibril pellet was resuspended in an equal volume of water. A second solution (70 μM α-synuclein in PBS) was then prepared, and a solution of these fibrils was added to a concentration of 2% (v/v) to seed the new solution. These samples were incubated at 37 °C for 12–24 h with vigorous agitation, yielding samples of F1 fibrils, essentially free from amorphous material, which were used immediately.

Fibril binding using ^{15}N–^{1}H NMR

The binding of α-synuclein fibrils to NbSyn2 was monitored using ^{15}N–^{1}H HSQC experiments following addition of between 1 and 4 molar equivalents of α-synuclein molecules in their fibrillar conformation to the ^{15}N-labeled NbSyn2.

Fibril binding using immunogold labeling and immunoelectron microscopy

The NbSyn2–fibril complex was obtained by the addition of NbSyn2 to α-synuclein fibrils in PBS, pH 7.5, with final concentrations of 0.15–1.5 and 70 μM, respectively. Charged carbon-coated nickel EM grids (400 mesh; Agar Scientific, Stansted, UK) were prepared for this study by the addition of 4 μl of the NbSyn2–α-synuclein complex in PBS. Samples were deposited onto grids immediately following dilution. Grids were washed three times with 10 μl H_2O, blocked with 15 μl of a 0.1% (w/v) filtered bovine serum albumin (BSA) solution in PBS for 20 min, and then incubated for 30 min with a monoclonal primary antibody recognizing the six-residue His-tag [Mouse anti-His (50 μg/μl), ZYMED Laboratories, San Francisco, CA, USA] diluted 250-fold in 0.1% BSA in PBS. The grids were blotted with filter paper between each washing step. Next, the grids were washed three times with 50 μl 0.1% BSA in PBS, for 5 min each time, before a 30-min incubation with goat anti-mouse 10 nm immunogold conjugate (GMHL10, BBInternational, Cardiff, UK), diluted 150-fold into 0.1% BSA in PBS. The grids were

washed with 3×50 μl 0.1% BSA in PBS, again for 5 min each time, then 3×50 μl H_2O, and negatively stained with 20 μl of uranyl acetate [2% (w/v) in H_2O; Agar Scientific]. Immunogold labeling was performed at room temperature and samples were viewed under 20,000–80,000× magnification at 80 kV excitation voltages using a Philips CM100 transmission electron microscope.

Accession numbers

Coordinates and structure factors have been deposited in the Protein Data Bank with accession number 2X6M.

Acknowledgements

E.D.G. acknowledges receipt of a long-term EMBO Fellowship and a Marie Curie Intra-European Fellowship. T.G. acknowledges the receipt of a studentship from the Parkinson's Disease Society. C.M.D. and J.C. acknowledge funding from the Wellcome and Leverhulme Trusts. S.-T.D.H. is a recipient of a Human Frontier Science Program Long-term Fellowship (LT0798/2005) and is supported in part by the National Science Council of the Republic of China, Taiwan (NSC97-2917-1-564-102). S.M. acknowledges the support of a Royal Society Dorothy Hodgkin Fellowship. M.D. is a research associate of the Belgian F.R.S-FNRS. N.C. is a recipient of a Human Frontier Science Program Long-term Fellowship (LT000795/2009). This work was further supported by the Vlaams Instituut voor Biotechnologie and by the Belgian Government under the framework of the Interuniversity Attraction Poles (I.A.P. P6/19). We thank the staff of the Biomolecular NMR Facility, Department of Chemistry, University of Cambridge, for their valuable assistance. We are grateful to the European Molecular Biology Laboratory for the use of beamline X11 at the Deutsches Elektronen-Synchrotron (Hamburg, Germany).

References

1. Chiti, F. & Dobson, C. M. (2006). Protein misfolding, functional amyloid, and human disease. *Annu. Rev. Biochem.* **75**, 333–366.
2. Baba, M., Nakajo, S., Tu, P. H., Tomita, T., Nakaya, K., Lee, V. M. *et al.* (1998). Aggregation of alpha-synuclein in Lewy bodies of sporadic Parkinson's disease and dementia with Lewy bodies. *Am. J. Pathol.* **152**, 879–884.
3. Cookson, M. R. (2005). The biochemistry of Parkinson's disease. *Annu. Rev. Biochem.* **74**, 29–52.
4. Moore, D. J., West, A. B., Dawson, V. L. & Dawson, T. M. (2005). Molecular pathophysiology of Parkinson's disease. *Annu. Rev. Neurosci.* **28**, 57–87.
5. Uversky, V. N. & Eliezer, D. (2009). Biophysics of Parkinson's disease: structure and aggregation of alpha-synuclein. *Curr. Protein Pept. Sci.* **10**, 483–499.
6. Waxman, E. A. & Giasson, B. I. (2009). Molecular mechanisms of alpha-synuclein neurodegeneration. *Biochim. Biophys. Acta*, **1792**, 616–624.
7. Chandra, S., Gallardo, G., Fernández-Chacón, R., Schlüter, O. M. & Südhof, T. C. (2005). Alpha-synuclein cooperates with CSPalpha in preventing neurodegeneration. *Cell*, **123**, 383–396.
8. Conway, K. A., Rochet, J. C., Bieganski, R. M. & Lansbury, P. T., Jr. (2001). Kinetic stabilization of the alpha-synuclein protofibril by a dopamine-alpha-synuclein adduct. *Science*, **294**, 1346–1349.
9. Rochet, J. C., Conway, K. A. & Lansbury, P. T., Jr. (2000). Inhibition of fibrillization and accumulation of prefibrillar oligomers in mixtures of human and mouse alpha-synuclein. *Biochemistry*, **39**, 10619–10626.
10. Conway, K. A., Lee, S. J., Rochet, J. C., Ding, T. T., Williamson, R. E. & Lansbury, P. T., Jr. (2000). Acceleration of oligomerization, not fibrillization, is a shared property of both alpha-synuclein mutations linked to early-onset Parkinson's disease: implications for pathogenesis and therapy. *Proc. Natl Acad. Sci. USA*, **97**, 571–576.
11. Volles, M. J. & Lansbury, P. T., Jr. (2003). Zeroing in on the pathogenic form of alpha-synuclein and its mechanism of neurotoxicity in Parkinson's disease. *Biochemistry*, **42**, 7871–7878.
12. Bodner, C. R., Maltsev, A. S., Dobson, C. M. & Bax, A. (2010). Differential phospholipid binding of alpha-synuclein variants implicated in Parkinson's disease revealed by solution NMR spectroscopy. *Biochemistry*, **49**, 862–871.
13. Bodner, C. R., Dobson, C. M. & Bax, A. (2009). Multiple tight phospholipid-binding modes of alpha-synuclein revealed by solution NMR spectroscopy. *J. Mol. Biol.* **390**, 775–790.
14. Lashuel, H. A., Hartley, D., Petre, B. M., Walz, T. & Lansbury, P. T., Jr. (2002). Neurodegenerative disease: amyloid pores from pathogenic mutations. *Nature*, **418**, 291.
15. Kim, H. Y., Cho, M. K., Kumar, A., Maier, E., Siebenhaar, C., Becker, S. *et al.* (2009). Structural properties of pore-forming oligomers of alpha-synuclein. *J. Am. Chem. Soc.* **131**, 17482–17489.
16. Caughey, B. & Lansbury, P. T. (2003). Protofibrils, pores, fibrils, and neurodegeneration: separating the responsible protein aggregates from the innocent bystanders. *Annu. Rev. Neurosci.* **26**, 267–298.
17. Tartaglia, G. G. & Vendruscolo, M. (2008). The Zyggregator method for predicting protein aggregation propensities. *Chem. Soc. Rev.* **37**, 1395–1401.
18. Bucciantini, M., Giannoni, E., Chiti, F., Baroni, F., Formigli, L., Zurdo, J. *et al.* (2002). Inherent toxicity of aggregates implies a common mechanism for protein misfolding diseases. *Nature*, **416**, 507–511.
19. Stefani, M. & Dobson, C. M. (2003). Protein aggregation and aggregate toxicity: new insights into protein folding, misfolding diseases and biological evolution. *J. Mol. Med.* **81**, 678–699.
20. Eliezer, D. (2009). Biophysical characterization of intrinsically disordered proteins. *Curr. Opin. Struct. Biol.* **19**, 23–30.

21. Dumoulin, M. & Dobson, C. M. (2004). Probing the origins, diagnosis and treatment of amyloid diseases using antibodies. *Biochimie*, **86**, 589–600.
22. Hamers-Casterman, C., Atarhouch, T., Muyldermans, S., Robinson, G., Hamers, C., Songa, E. B. *et al.* (1993). Naturally occurring antibodies devoid of light chains. *Nature*, **363**, 446–448.
23. Muyldermans, S., Baral, T. N., Retamozzo, V. C., De Baetselier, P., De Genst, E., Kinne, J. *et al.* (2009). Camelid immunoglobulins and nanobody technology. *Vet. Immunol. Immunopathol.* **128**, 178–183.
24. De Genst, E., Saerens, D., Muyldermans, S. & Conrath, K. (2006). Antibody repertoire development in camelids. *Dev. Comp. Immunol.* **30**, 187–198.
25. Holliger, P. & Hudson, P. J. (2005). Engineered antibody fragments and the rise of single domains. *Nat. Biotechnol.* **23**, 1126–1136.
26. Muyldermans, S., Cambillau, C. & Wyns, L. (2001). Recognition of antigens by single-domain antibody fragments: the superfluous luxury of paired domains. *Trends Biochem. Sci.* **26**, 230–235.
27. Chan, P. H., Pardon, E., Menzer, L., De Genst, E., Kumita, J. R., Christodoulou, J. *et al.* (2008). Engineering a camelid antibody fragment that binds to the active site of human lysozyme and inhibits its conversion into amyloid fibrils. *Biochemistry*, **47**, 11041–11054.
28. Dumoulin, M., Last, A. M., Desmyter, A., Decanniere, K., Canet, D., Larsson, G. *et al.* (2003). A camelid antibody fragment inhibits the formation of amyloid fibrils by human lysozyme. *Nature*, **424**, 783–788.
29. Koide, S. (2009). Engineering of recombinant crystallization chaperones. *Curr. Opin. Struct. Biol.* **19**, 449–457.
30. Messer, A., Lynch, S. M. & Butler, D. C. (2009). Developing intrabodies for the therapeutic suppression of neurodegenerative pathology. *Expert Opin. Biol. Ther.* **9**, 1189–1197.
31. Kirchhofer, A., Helma, J., Schmidthals, K., Frauer, C., Cui, S., Karcher, A. *et al.* (2010). Modulation of protein properties in living cells using nanobodies. *Nat. Struct. Mol. Biol.* **17**, 133–138.
32. Paik, S. R., Shin, H. J., Lee, J. H., Chang, C. S. & Kim, J. (1999). Copper(II)-induced self-oligomerization of alpha-synuclein. *Biochem. J.* **340**, 821–828.
33. Uversky, V. N., Li, J. & Fink, A. L. (2001). Metal-triggered structural transformations, aggregation, and fibrillation of human alpha-synuclein. A possible molecular NK between Parkinson's disease and heavy metal exposure. *J. Biol. Chem.* **276**, 44284–44296.
34. Binolfi, A., Rasia, R. M., Bertoncini, C. W., Ceolin, M., Zweckstetter, M., Griesinger, C. *et al.* (2006). Interaction of alpha-synuclein with divalent metal ions reveals key differences: a link between structure, binding specificity and fibrillation enhancement. *J. Am. Chem. Soc.* **128**, 9893–9901.
35. Binolfi, A., Lamberto, G. R., Duran, R., Quintanar, L., Bertoncini, C. W., Souza, J. M. *et al.* (2008). Site-specific interactions of Cu(II) with alpha and beta-synuclein: bridging the molecular gap between metal binding and aggregation. *J. Am. Chem. Soc.* **130**, 11801–11812.
36. Antony, T., Hoyer, W., Cherny, D., Heim, G., Jovin, T. M. & Subramaniam, V. (2003). Cellular polyamines promote the aggregation of alpha-synuclein. *J. Biol. Chem.* **278**, 3235–3240.
37. Goers, J., Uversky, V. N. & Fink, A. L. (2003). Polycation-induced oligomerization and accelerated fibrillation of human alpha-synuclein in vitro. *Protein Sci.* **12**, 702–707.
38. Hoyer, W., Cherny, D., Subramaniam, V. & Jovin, T. M. (2004). Impact of the acidic C-terminal region comprising amino acids 109–140 on alpha-synuclein aggregation in vitro. *Biochemistry*, **43**, 16233–16242.
39. Hoyer, W., Cherny, D., Subramaniam, V. & Jovin, T. M. (2004). Rapid self-assembly of alpha-synuclein observed by in situ atomic force microscopy. *J. Mol. Biol.* **340**, 127–139.
40. Fernández, C. O., Hoyer, W., Zweckstetter, M., Jares-Erijman, E. A., Subramaniam, V., Griesinger, C. & Jovin, T. M. (2004). NMR of alpha-synuclein–polyamine complexes elucidates the mechanism and kinetics of induced aggregation. *EMBO J.* **23**, 2039–2046.
41. Rivers, R. C., Kumita, J. R., Tartaglia, G. G., Dedmon, M. M., Pawar, A., Vendruscolo, M. *et al.* (2008). Molecular determinants of the aggregation behavior of alpha- and beta-synuclein. *Protein Sci.* **17**, 887–898.
42. Bertoncini, C. W., Jung, Y. S., Fernandez, C. O., Hoyer, W., Griesinger, C., Jovin, T. M. & Zweckstetter, M. (2005). Release of long-range tertiary interactions potentiates aggregation of natively unstructured alpha-synuclein. *Proc. Natl Acad. Sci. USA*, **102**, 1430–1435.
43. Dedmon, M. M., Lindorff-Larsen, K., Christodoulou, J., Vendruscolo, M. & Dobson, C. M. (2005). Mapping long-range interactions in alpha-synuclein using spin-label NMR and ensemble molecular dynamics simulations. *J. Am. Chem. Soc.* **127**, 476–477.
44. Rospigliosi, C. C., McClendon, S., Schmid, A. W., Ramlall, T. F., Barré, P., Lashuel, H. A. & Eliezer, D. (2009). E46K Parkinson's-linked mutation enhances C-terminal-to-N-terminal contacts in alpha-synuclein. *J. Mol. Biol.* **388**, 1022–1032.
45. Rekas, A., Adda, C. G., Andrew Aquilina, J., Barnham, K. J., Sunde, M., Galatis, D. *et al.* (2004). Interaction of the molecular chaperone alphaB-crystallin with alpha-synuclein: effects on amyloid fibril formation and chaperone activity. *J. Mol. Biol.* **340**, 1167–1183.
46. Dedmon, M. M., Christodoulou, J., Wilson, M. R. & Dobson, C. M. (2005). Heat shock protein 70 inhibits alpha-synuclein fibril formation via preferential binding to prefibrillar species. *J. Biol. Chem.* **280**, 14733–14740.
47. Grimminger-Marquardt, V. & Lashuel, H. A. (2010). Structure and function of the molecular chaperone Hsp104 from yeast. *Biopolymers*, **93**, 252–276.
48. Dumoulin, M., Conrath, K., Van Meirhaeghe, A., Meersman, F., Heremans, K., Frenken, L. G. *et al.* (2002). Single-domain antibody fragments with high conformational stability. *Protein Sci.* **11**, 500–515.
49. Kumar, M. D. & Gromiha, M. M. (2006). PINT: protein–protein interactions thermodynamic database. *Nucleic Acids Res.* **34**, D195–D198.
50. Velázquez-Campoy, A., Ohtaka, H., Nezami, A., Muzammil, S. & Freire, E. (2004). Isothermal titration calorimetry.*Curr. Protoc. Cell. Biol.*; Chapter 17, Unit. 17, 8.

51. Evans, J. (1995). pp. 44, 1st edit. Oxford University Press, Oxford, UK.
52. Bermel, W., Bertini, I., Felli, I. C., Lee, Y. M., Luchinat, C. & Pierattelli, R. (2006). Protonless NMR experiments for sequence-specific assignment of backbone nuclei in unfolded proteins. *J. Am. Chem. Soc.* **128**, 3918–3919.
53. Murphy, K. P. & Freire, E. (1992). Thermodynamics of structural stability and cooperative folding behavior in proteins. *Adv. Protein Chem.* **43**, 313–361.
54. Vuchelen, A., O'Day, E., De Genst, E., Pardon, E., Wyns, L., Dumoulin, M. *et al.* (2009). (1)H, (13)C and (15)N assignments of a camelid nanobody directed against human alpha-synuclein. *Biomol. NMR Assign.* **3**, 231–233.
55. Padlan, E. A. (1994). Anatomy of the antibody molecule. *Mol. Immunol.* **31**, 169–217.
56. Cavanagh, J., Fairbrother, W. J., Palmer, A. G., III, Rance, M. & Skelton, N. J. (2007). pp. 725,, 2nd edit. Elsevier Academic Press, USA, Boston, MA.
57. Ban, T., Hamada, D., Hasegawa, K., Naiki, H. & Goto, Y. (2003). Direct observation of amyloid fibril growth monitored by thioflavin T fluorescence. *J. Biol. Chem.* **278**, 16462–16465.
58. Matulis, D. & Lovrien, R. E. (1998). 1-Anilino-8-naphtalene sulphonate anion-protein binding depends primarily on ion-pair formation. *Biophys. J.* **74**, 422–429.
59. Stanfield, R. L. & Wilson, I. A. (1995). Protein–peptide interactions. *Curr. Opin. Struct. Biol.* **5**, 103–113.
60. Jaya, N., Garcia, V. & Vierling, E. (2009). Substrate binding site flexibility of the small heat shock protein molecular chaperones. *Proc. Natl Acad. Sci. USA*, **106**, 15604–15609.
61. Chen, D. H., Luke, K., Zhang, J., Chiu, W. & Wittung-Stafshede, P. (2008). Location and flexibility of the unique C-terminal tail of *Aquifex aeolicus* co-chaperonin protein 10 as derived by cryo-electron microscopy and biophysical techniques. *J. Mol. Biol.* **381**, 707–717.
62. Lindner, R. A., Kapur, A., Mariani, M., Titmuss, S. J. & Carver, J. A. (1998). Structural alterations of alpha-crystallin during its chaperone action. *Eur. J. Biochem.* **258**, 170–183.
63. Pineda, J. R., Callender, R. & Schwartz, S. D. (2007). Ligand binding and protein dynamics in lactate dehydrogenase. *Biophys. J.* **93**, 1474–1483.
64. Vilar, M., Chou, H. T., Lührs, T., Maji, S. K., Riek-Loher, D., Verel, R. *et al.* (2008). The fold of alpha-synuclein fibrils. *Proc. Natl Acad. Sci. USA*, **105**, 8637–8642.
65. Qin, Z., Hu, D., Han, S., Hong, D. P. & Fink, A. L. (2007). Role of different regions of alpha-synuclein in the assembly of fibrils. *Biochemistry*, **46**, 13322–13330.
66. Lauwereys, M., Arbabi Ghahroudi, M., Desmyter, A., Kinne, J., Hölzer, W., De Genst, E. *et al.* (1998). Potent enzyme inhibitors derived from dromedary heavy-chain antibodies. *EMBO J.* **17**, 3512–3520.
67. Conrath, K. E., Lauwereys, M., Galleni, M., Matagne, A., Frere, J. M., Kinne, J. *et al.* (2001). Beta-lactamase inhibitors derived from single-domain antibody fragments elicited in the camelidae. *Antimicrob. Agents Chemother.* **45**, 2807–2812.
68. Hoyer, W., Antony, T., Cherny, D., Heim, G., Jovin, T. M. & Subramaniam, V. (2002). *J. Mol. Biol.* **322**, 383–393.
69. Leslie, A. G. (2006). The integration of macromolecular diffraction data. *Acta Crystallogr., Sect. D: Biol. Crystallogr.* **62**, 48–57.
70. Evans, P. (2006). Scaling and assessment of data quality. *Acta Crystallogr., Sect. D: Biol. Crystallogr.* **62**, 72–82.
71. Storoni, L. C., McCoy, A. J. & Read, R. J. (2004). Likelihood-enhanced fast rotation functions. *Acta Crystallogr., Sect. D: Biol. Crystallogr.* **60**, 432–438.
72. Spinelli, S., Frenken, L., Bourgeois, D., de Ron, L., Bos, W., Verrips, T. *et al.* (1996). The crystal structure of a llama heavy chain variable domain. *Nat. Struct. Biol.* **3**, 752–757.
73. Perrakis, A., Morris, R. & Lamzin, V. S. (1999). Automated protein model building combined with iterative structure refinement. *Nat. Struct. Biol.* **6**, 458–463.
74. Murshudov, G. N., Vagin, A. A. & Dodson, E. J. (1997). Refinement of macromolecular structures by the maximum-likelihood method. *Acta Crystallogr., Sect. D: Biol. Crystallogr.* **53**, 240–255.
75. Emsley, P. & Cowtan, K. (2004). Coot: model-building tools for molecular graphics. *Acta Crystallogr., Sect. D: Biol. Crystallogr.* **60**, 2126–2132.
76. Reynolds, C., Damerell, D. & Jones, S. (2009). ProtorP: a protein–protein interaction analysis server. *Bioinformatics*, **25**, 413–414.
77. Delaglio, F., Grzesiek, S., Vuister, G. W., Zhu, G., Pfeifer, J. & Bax, A. (1995). NMRPipe: a multidimensional spectral processing system based on UNIX pipes. *J. Biomol. NMR*, **6**, 277–293.
78. Goddard, T. D. & Kneller, D. G. SPARKY 3, University of California, San Francisco